Hindawi
Journal of Sensors
Volume 2021, Article ID 5539302, 14 pages
https://doi.org/10.1155/2021/5539302

Research Article

A Method to Locate Tree Positions Using Ultrawideband Technology

Fangxing Yuan,[1,2] Sheng Chen,[3] Luming Fang,[1,2] Siqing Zheng,[1,2] Yuzhen Liu,[1,2] and Junjun Ren[1,2]

[1]*Key Laboratory of Forestry Intelligent Monitoring and Information Technology Research of Zhejiang Province, Zhejiang A & F University, Lin'an, 311300 Zhejiang, China*
[2]*College of Information Engineering, Zhejiang A & F University, Lin'an, 311300 Zhejiang, China*
[3]*Zhejiang Forest Resources Monitoring Center, Hangzhou, 310004 Zhejiang, China*

Correspondence should be addressed to Luming Fang; flming@zafu.edu.cn

Received 24 January 2021; Revised 30 April 2021; Accepted 21 May 2021; Published 6 July 2021

Academic Editor: Bahareh Kalantar

Tree position plays an important role in research on forest resources and ecological functions, and quickly and accurately obtaining tree position data has long been the focus of investigators. However, the classical method is time-consuming and laborious; thus, a convenient method of measuring tree position is needed. The primary achievements of this study include the following: (1) a device was designed for precise location of trees; (2) a new location algorithm was proposed for pentagonal localization based on the received signal strength indication and ultrawideband technology; and (3) a PC software application was developed for automatically storing and uploading tree position data. The device was applied to 10 circular plots with a diameter of 24 m to test the positioning speed and accuracy. The results showed that the tree positions could be accurately estimated. On the x- and y-axes, the biases were -3.94 and 3.36 cm, respectively, and the root mean square errors (RMSEs) were 28.39 and 28.53 cm, respectively. The mean error (Ed) between the estimated and reference distances was 36.13 cm, and the standard deviation was 16.67 cm. The device is inexpensive and easy to use and carry in the field; thus, it is suitable for locating trees in environments with complex terrain.

1. Introduction

Tree position measurements are of great significance in forest resource investigations. The rapid and accurate acquisition of tree position in sample plots is helpful for predicting the growth of tree DBH and population development trends and has important ecological significance for revealing the relationship between trees and tree species [1, 2]. Traditional measurements use a box compass combined with tapes or a laser distance meter. The measurement process is time-consuming and laborious, and the data are read and recorded manually, which is inefficient and easily confounded, thus seriously restricting the quality and efficiency of acquiring tree positions in sample field surveys [3–7]. Developing a method of improving the quality and efficiency of tree position information acquisition has long been an issue for forestry researchers [8–10].

In recent years, many devices and methods have been developed for locating trees in sample plots. The Haglöf Postex® Laser uses ultrasonic solution for tree position measurement; however, due to the short distance of ultrasonic measurement, the size of the sample plot will be limited [11]. The global navigation satellite system (GNSS) [12–15] can provide positioning coordinate information in most environments. However, signal attenuation or even signal disappearance occurs in stands with high canopy density, which is also greatly affected by the density of trees in the sample plot [16–18]. Total stations are a type of precise electronic survey system with a mapping instrument that integrates rangefinders, electronic theodolites, and microprocessors [19]. Such systems provide an effective method for locating trees on the sample plot but have some disadvantages, such as inconvenience, complicated operation, and expensive price. Terrestrial laser scanning

(TLS), also known as ground-based light detection and ranging (LiDAR) [20–24], has been applied for the extraction of various forestry attributes [25–28]; however, due to some operational and performance limitations, laborious carrying and installation, and complex data processing, TLS cannot be widely used [29, 30]. Close-range photogrammetry (CRP) [31–33] and smartphones with time of flight (TOF) [34–36] cameras have also been applied to obtain tree locations; however, they are highly susceptible to stand density, surface vegetation, and light intensity and require specialized knowledge to handle complex point cloud computing [37]. Therefore, there are some limitations to applying these devices and methods for determining the position of trees.

Advances in sensing technology have led to the development of devices for precisely locating trees in the field. Ultrawideband (UWB) technology [38–42] is a kind of communication technology that uses discontinuous less-than-nanosecond pulses without carriers and has the advantages of a high transmission rate, strong multipath resolution, strong anti-interference ability, and strong penetration ability. It has been widely used in the determination of distance and position. Compared with other wireless communication technologies (Wi-Fi, ZigBee, etc.), it has higher precision [43–45].

In this paper, a measurement device using UWB sensors was developed for accurate positioning, rapid measurement recording, automatic transmission, and processing of trees, and it has the advantages of low cost and ease of carrying.

2. System Design

2.1. Design of the Main Device. The device is mainly composed of a base station and a mobile station, as shown in Figure 1. The base station consists of a supporting tripod and five 1 m long poles with a UWB module on top. The poles and supporting tripod can be folded and shrunk, which facilitates the carrying of the device by survey crews in the field. Mobile station is the location tag. Table 1 describes the components used by the device and their main properties. The circuit of the base station is mainly composed of a microprocessor, power module, gyroscope module, compass module, UWB module, and display screen. The circuit of the mobile station is mainly composed of a microprocessor, power module, UWB module, secure digital memory card (SD card), Bluetooth module, button, and display screen. The device uses an 8-bit microprocessor, which is high speed and low cost and has strong anti-interference. The power module is composed of a lithium battery, a power management chip, and a switch. The lithium battery is used as the supply power to the system components, and the power management chip can protect the lithium battery and other circuits from overcurrent. The gyroscope module is used to collect the location information of the base station. The compass module is used to collect the azimuth information. The base station is equipped with five UWB modules, and the mobile station is equipped with one UWB module

Figure 1: Main device and its components: 1: display panel; 2: keys; 3: UWB casings; 4: metal folding pieces; 5: carbon fibers; 6: fixing knobs; 7: printed circuit board (PCB); 8: level adjusting knob; 9: rotary locks; 10: fixing card buckle; 11: limit card buckles; 12: rubber pads.

to measure the distance between the mobile station and the base station. The display screen displays the measurement information, the SD card stores the distance and location coordinate data collected by the mobile station, and the Bluetooth module transmits the data between the mobile station and host computer.

2.2. Principle of UWB Ranging. To accurately measure the distances, the UWB sensor based on the double-sided two-way ranging (DS-TWR) principle [46, 47] was selected. Due to the error introduced by clock deviation in single-sided two-way ranging (SS-TWR) [48, 49] measurement, DS-TWR adds another round of communication on the basis of SS-TWR to compensate for the error introduced through two communication times and increase the accuracy of ranging. The principle is shown in Figure 2, and the formula is shown in

$$D = c \times T_{\text{prop}} = c \times \frac{T_{\text{round1}} \times T_{\text{round2}} - T_{\text{reply1}} \times T_{\text{reply2}}}{T_{\text{round1}} + T_{\text{round2}} + T_{\text{reply1}} + T_{\text{reply2}}}, \quad (1)$$

where Node A and Node B are communication nodes, D is the distance between Node A and Node B, T_{prop} is the time for the wireless pulse signal to travel in the air, c is the speed of light, T_{round1} is the total time of Node A receiving and sending pulses in the first round of communication, T_{reply1} is the waiting time of Node B in the first round of communication, T_{round2} is the total time required for Node B to receive and send pulses in the second round of communication, and T_{reply2} is the waiting time of Node A in the second round of communication.

2.3. Design of Software Process. The software was designed to acquire the distances between the base station and the mobile

Table 1: Descriptive statistics of the device's components[1].

Component	Chip model/type	Interface type	Parameter	Function
Microprocessor	STC15W4K56S4	Digital, serial port, SPI, etc.	SRAM: 4 KB; flash: 56 KB data processing	Microprocessor
Power management circuit	TP4056, AMS1117, etc.	Digital, power	Input: 3.7 V-4.2 V, 5 V; output: 5 V, 3.3 V	Power management
Battery	Lithium battery	Power	4000 mAh	Power supply
Gyroscope module	JY901B	Serial port	Resolution: 0.01°	Attitude measurement
Compass module	GY-26	Serial port	Resolution: 0.1°	Azimuth measurement
UWB module	D-DWM-PG1.7	Serial port	Resolution: 1 cm; range: 0-50 m	Distance measurement
Display	OLED	SPI	128 × 64 pixels	Data display
Keyboard	PVC	Digital	6 keys	Data recording
SD card	Micro SD	SPI	2 GB	Data storage
Bluetooth	HC-06	Serial port	Range: 0-15 m	COMM with upper computer

[1]SPI: serial peripheral interface; SRAM: static random-access memory; KB: kilobyte; V: voltage; mAh: milliampere-hour; GB: gigabyte; COMM: communication.

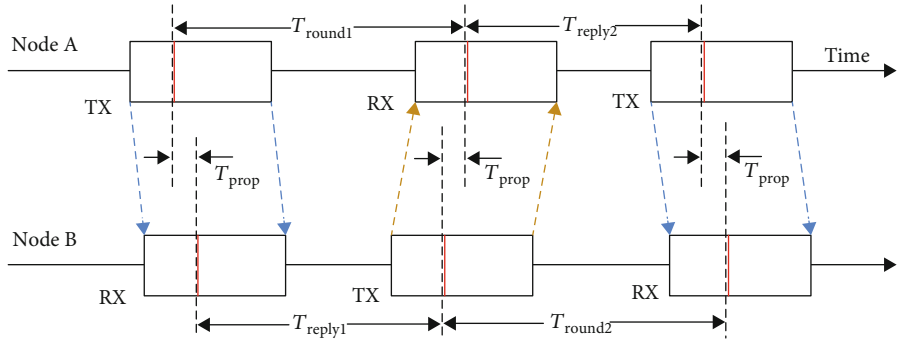

Figure 2: Scheme of double-sided, two-way ranging (DS-TWR).

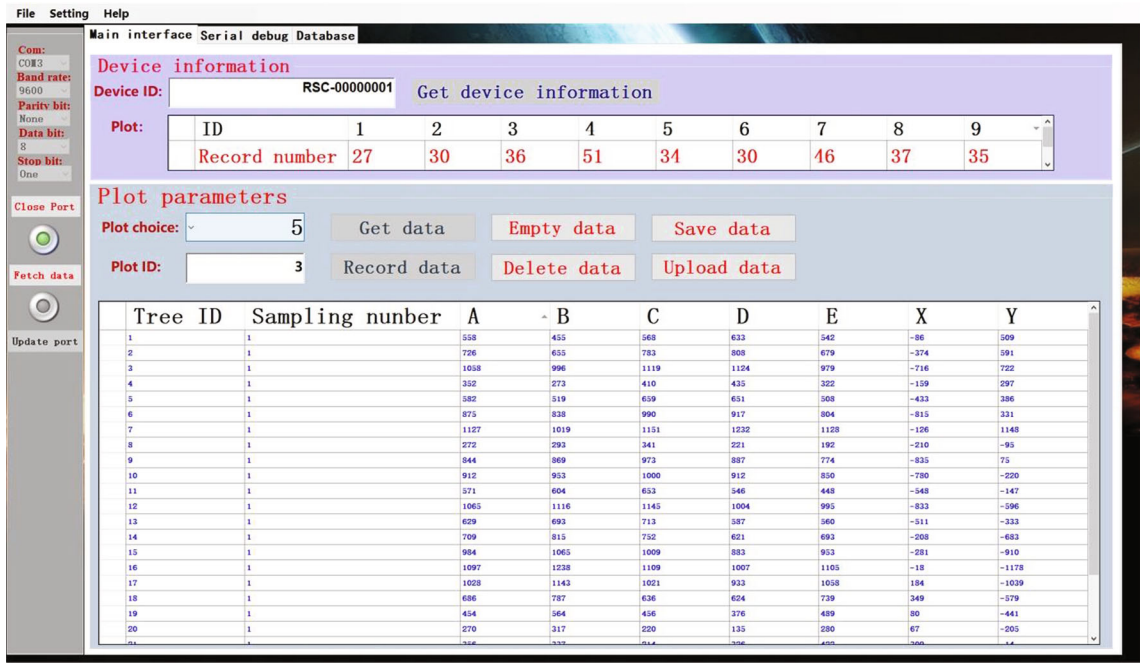

Figure 3: Host computer interface.

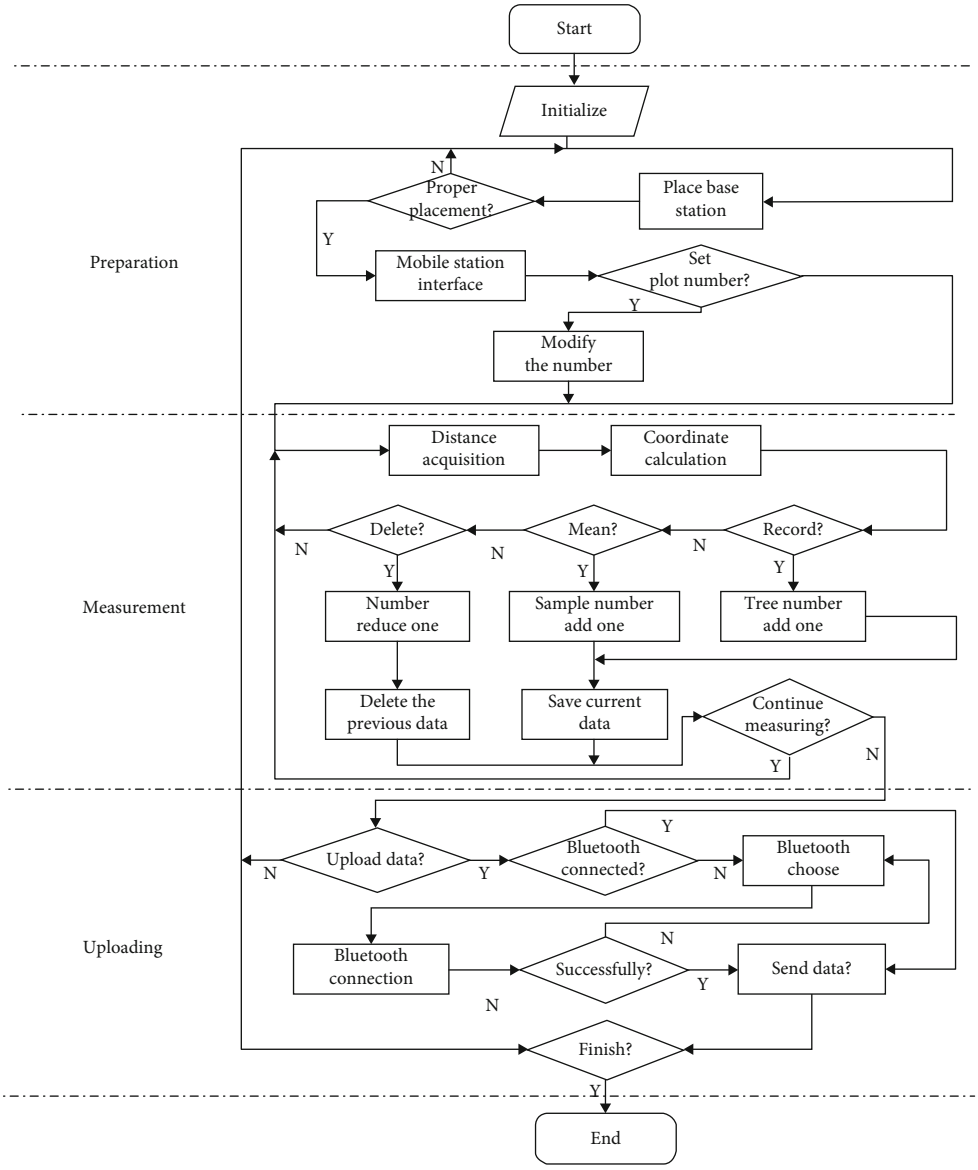

Figure 4: Flowchart of the system.

station and to calculate the positioning coordinates, key control, and data management, as shown in Figure 3. The GUI enables investigators to read device information, calculate data statistics, and export data to facilitate data processing and analysis. The general flow of the software is shown in Figure 4, which is divided into three stages: preparation, measurement, and upload. During the measurement, the tree number and the corresponding position information can be automatically completed.

3. Materials and Methods

3.1. Study Area. The test site chosen here was Zhejiang A and F University, Hangzhou, China (30°15′N, 119°43′E). A total of 10 circular plots with a diameter of 24 m (371 trees in total) were measured (a circular plot with a radius of 11.28 m is usually used in forest surveys in South China; therefore, we set the radius as 12 m). The surfaces were mainly covered by leaf litter in plots 1 to 6 and denser weeds in plots 7 to 10 (Table 2).

3.2. Methods

3.2.1. Measurement Process Design. To test the positioning accuracy, the reference data measured using theodolite with a laser rangefinder were compared with the data measured by the device. All measurements used the local east, north, up (ENU) coordinate system. The measurement operation for theodolite with a laser rangefinder and the device are shown in Figures 5 and 6, respectively. Poles B and C of the device pointing to the north and east were the positive *y*-

Table 2: Descriptive statistics of the sample plot[2].

Plot	Number of trees	Dominant species	Slope (°)
1	27	S1	0.9
2	30	S1, S2, S3	1.9
3	36	S1, S3, S4, S5, S6	4.8
4	51	S3, S4, S11, S12	5.8
5	34	S3, S5, S6	2.5
6	30	S1, S3, S6	4.9
7	45	S1, S3, S4, S7	12.6
8	37	S5, S8, S9	14.1
9	35	S3, S4, S5, S10, S13	13.8
10	46	S5, S10, S13	12.1

[2]S1: *soapberry*; S2: *southern magnolia*; S3: *camphor tree*; S4: *tulip tree*; S5: *Michelia alba*; S6: *pine tree*; S7: *Dalbergia hupeana*; S8: *Ormosia hosiei*; S9: *Ginkgo biloba*; S10: *Chinese parasol*; S11: *Michelia maudiae*; S12: *Celtis sinensis*; S13: *Zelkova schneideriana*.

Figure 5: The theodolite with a laser rangefinder measurement.

and x-axes, respectively. Pole A was the positive z-axis. The device measurement process was as follows.

(1) The base station was placed in the center of the circle plot. According to the gyroscope data, the station was adjusted to the horizontal position and then pole B was moved to the north according to the compass data

(2) The plot ID was set on the mobile station

(3) We placed the mobile station at the measuring position of the trees (1.3 m above the ground), pressed the record button, and recorded the position data. To ensure that the measured value is close to the reference value, the survey crew can press the average key for multiple samplings. Finally, the average value is automatically calculated. The actual operation is shown in Figure 7

Figure 6: Placement of the device.

Figure 7: Position of the tree. On the display screen, 1 is the tree code and sampling number, 2 is the coordinates, 3 is the distances between the base stations and the mobile station, 4 is the delete key, 5 is the page key, 6 is the record key, and 7 is the average key.

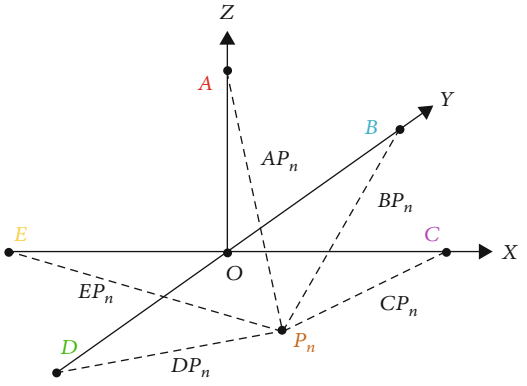

Figure 8: A diagram of pentagonal localization. $|OA| = |OB| = |OC| = |OD| = |OE| = 1$ m.

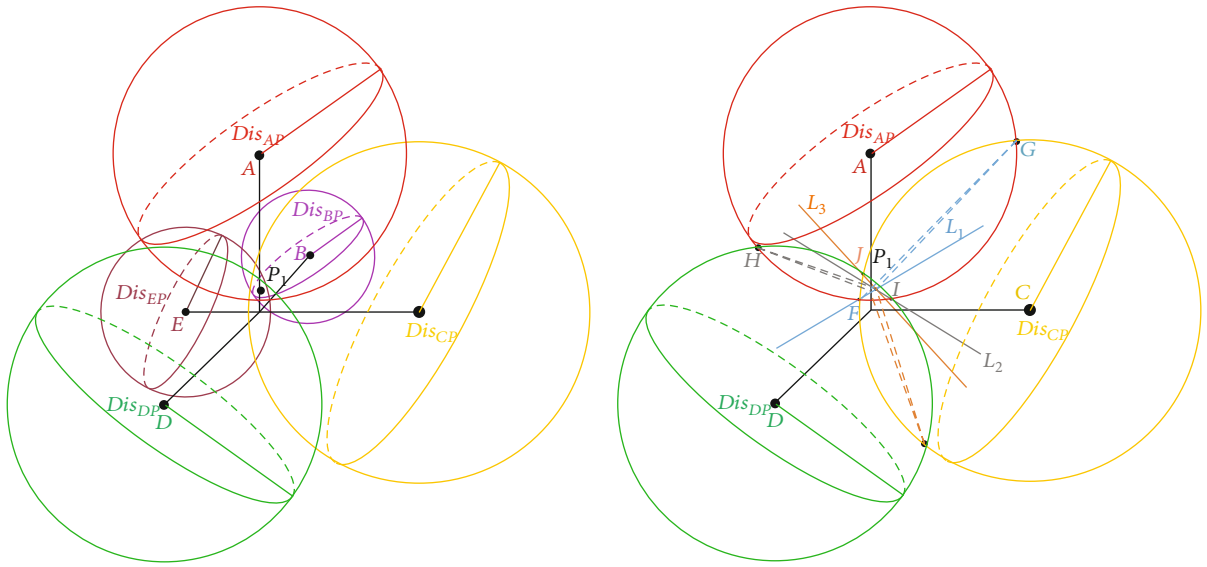

Figure 9: Position estimation using (a) pentagonal localization and (b) trilateration localization.

(4) After measuring the position of trees in the plot, the data were uploaded to the host computer for statistical analysis

3.2.2. Estimation Method of Tree Position. The distances between P_n and each antenna anchor point are shown in Figure 8.

Taking OC as the positive x-axis, OB as the positive y-axis, and OA as the positive z-axis, the coordinates of points A–E can be obtained:

$$\begin{aligned}(X_A, Y_A, Z_A) &= (0, 0, 1),\\ (X_B, Y_B, Z_B) &= (0, 1, 0),\\ (X_C, Y_C, Z_C) &= (1, 0, 0),\\ (X_D, Y_D, Z_D) &= (0, -1, 0),\\ (X_E, Y_E, Z_E) &= (-1, 0, 0).\end{aligned} \tag{2}$$

Assuming that the P_n coordinates are (X_n, Y_n, Z_n), the distance between P_n and each anchor point is as follows:

$$\begin{aligned}AP_n &= \sqrt{(X_n - X_A)^2 + (Y_n - Y_A)^2 + (Z_n - Z_A)^2}\\ &= \sqrt{X_n{}^2 + Y_n{}^2 + (Z_n - 1)^2},\end{aligned} \tag{3}$$

$$\begin{aligned}BP_n &= \sqrt{(X_n - X_B)^2 + (Y_n - Y_B)^2 + (Z_n - Z_B)^2}\\ &= \sqrt{X_n{}^2 + (Y_n - 1)^2 + Z_n{}^2},\end{aligned} \tag{4}$$

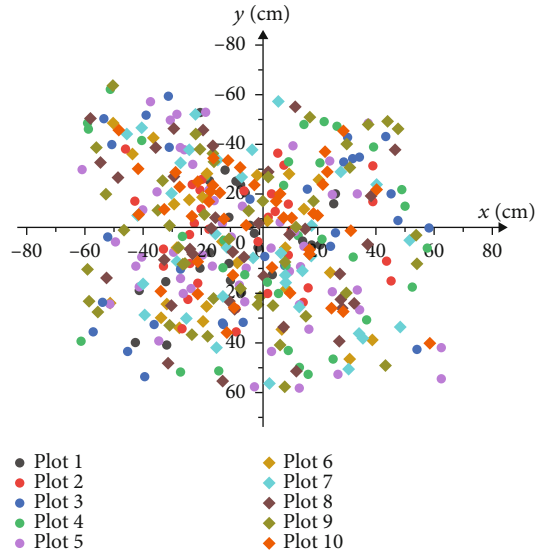

Figure 10: Errors measured by the device.

$$\begin{aligned}CP_n &= \sqrt{(X_n - X_C)^2 + (Y_n - Y_C)^2 + (Z_n - Z_C)^2}\\ &= \sqrt{(X_n - 1)^2 + Y_n{}^2 + Z_n{}^2},\end{aligned} \tag{5}$$

$$\begin{aligned}DP_n &= \sqrt{(X_n - X_D)^2 + (Y_n - Y_D)^2 + (Z_n - Z_D)^2}\\ &= \sqrt{X_n{}^2 + (Y_n + 1)^2 + Z_n{}^2},\end{aligned} \tag{6}$$

$$EP_n = \sqrt{(X_n - X_E)^2 + (Y_n - Y_E)^2 + (Z_n - Z_E)^2} = \sqrt{(X_n + 1)^2 + {Y_n}^2 + {Z_n}^2}. \quad (7)$$

In Equations (3)–(7), any four equations can be used to determine the P_n coordinates.

As shown in Figure 9(a), in practical applications, the UWB wireless signal will be obstructed and experience interference by the surrounding environment, such as the trunks, branches, and leaves, resulting in signal attenuation [50, 51] and slightly longer communication time; therefore, the AP_n, BP_n, CP_n, DP_n, and EP_n values are slightly greater than the actual values and do not intersect at a common point. To achieve accurate positioning and mitigate the influence of signal attenuation on ranging, some scholars have proposed using trilateration and quadrilateral localization for corresponding positioning depending on the received signal strength indication (RSSI) [52, 53].

According to the principles of trilateration [54, 55] and quadrilateral localization [56], 10 sets of pairwise intersecting spheres can be developed from Figure 9(a) for triangular localization. Take Figure 9(b) as an example, where three spheres A, C, and D intersect in pairs and the intersection is three planes (FGP_1, HIP_1, and JKP_1). The plane equation can be obtained by subtracting Equations (3), (5), and (6) in pairs:

$$\begin{aligned}
&2(X_C - X_A)X_n + 2(Y_C - Y_A)Y_n + 2(Z_C - Z_A)Za_n = {AP_n}^2 + {X_C}^2 + {Y_C}^2 + {Z_C}^2 - {CP_n}^2 - {X_A}^2 - {Y_A}^2 - {Z_A}^2,\\
&2(X_D - X_A)X_n + 2(Y_D - Y_A)Y_n + 2(Z_D - Z_A)Z_n = {AP_n}^2 + {X_D}^2 + {Y_D}^2 + {Z_D}^2 - {DP_n}^2 - {X_A}^2 - {Y_A}^2 - {Z_A}^2,\\
&2(X_D - X_C)X_n + 2(Y_D - Y_C)Y_n + 2(Z_D - Z_C)Z_n = {CP_n}^2 + {X_D}^2 + {Y_D}^2 + {Z_D}^2 - {DP_n}^2 - {X_C}^2 - {Y_C}^2 - {Z_C}^2.
\end{aligned} \quad (8)$$

In addition, because the three planes intersect in pairs, three lines L_1, L_2, and L_3 can be obtained by pairwise combination in Equation (8). The three lines intersect at point P_1, and the coordinates of $P_1\,(X_1, Y_1, Z_1)$ can be obtained according to Equation (8). In the same way, the coordinates of the other nine combinations can be obtained: $P_2\,(X_2, Y_2, Z_2)$, $P_3\,(X_3, Y_3, Z_3)$, $P_4\,(X_4, Y_4, Z_4)$, $P_5\,(X_5, Y_5, Z_5)$, $P_6\,(X_6, Y_6, Z_6)$, $P_7\,(X_7, Y_7, Z_7)$, $P_8\,(X_8, Y_8, Z_8)$, $P_9\,(X_9, Y_9, Z_9)$, and $P_{10}\,(X_{10}, Y_{10}, Z_{10})$. As trees are located according to two-dimensional coordinates [33, 57], the coordinates of $P_n\,(X_n, Y_n)$ only need to be obtained to locate trees in the sample plot:

$$\begin{aligned}
X_n &= \frac{\left(X_1/\left({AP_n}^2 + {BP_n}^2 + {CP_n}^2\right)\right) + \left(X_2/\left({AP_n}^2 + {BP_n}^2 + {DP_n}^2\right)\right) + \left(X_3/\left({AP_n}^2 + {BP_n}^2 + {EP_n}^2\right)\right) + \left(X_4/\left({AP_n}^2 + {CP_n}^2 + {DP_n}^2\right)\right) + \left(X_5/\left({AP_n}^2 + {CP_n}^2 + {EP_n}^2\right)\right)}{\left(1/\left({AP_n}^2 + {BP_n}^2 + {CP_n}^2\right)\right) + \left(1/\left({AP_n}^2 + {BP_n}^2 + {DP_n}^2\right)\right) + \left(1/\left({AP_n}^2 + {BP_n}^2 + {EP_n}^2\right)\right) + \left(1/\left({AP_n}^2 + {CP_n}^2 + {DP_n}^2\right)\right) + \left(1/\left({AP_n}^2 + {CP_n}^2 + {EP_n}^2\right)\right)} \\
&\quad + \frac{\left(X_6/\left({AP_n}^2 + {DP_n}^2 + {EP_n}^2\right)\right) + \left(X_7/\left({BP_n}^2 + {CP_n}^2 + {DP_n}^2\right)\right) + \left(X_8/\left({BP_n}^2 + {CP_n}^2 + {EP_n}^2\right)\right) + \left(X_9/\left({BP_n}^2 + {DP_n}^2 + {EP_n}^2\right)\right) + \left(X_{10}/\left({CP_n}^2 + {DP_n}^2 + {EP_n}^2\right)\right)}{+\left(1/\left({AP_n}^2 + {DP_n}^2 + {EP_n}^2\right)\right) + \left(1/\left({BP_n}^2 + {CP_n}^2 + {DP_n}^2\right)\right) + \left(1/\left({BP_n}^2 + {CP_n}^2 + {EP_n}^2\right)\right) + \left(1/\left({BP_n}^2 + {DP_n}^2 + {EP_n}^2\right)\right) + \left(1/\left({CP_n}^2 + {DP_n}^2 + {EP_n}^2\right)\right)} \\
Y_n &= \frac{\left(Y_1/\left({AP_n}^2 + {BP_n}^2 + {CP_n}^2\right)\right) + \left(Y_2/\left({AP_n}^2 + {BP_n}^2 + {DP_n}^2\right)\right) + \left(Y_3/\left({AP_n}^2 + {BP_n}^2 + {EP_n}^2\right)\right) + \left(Y_4/\left({AP_n}^2 + {CP_n}^2 + {DP_n}^2\right)\right) + \left(Y_5/\left({AP_n}^2 + {CP_n}^2 + {EP_n}^2\right)\right)}{\left(1/\left({AP_n}^2 + {BP_n}^2 + {CP_n}^2\right)\right) + \left(1/\left({AP_n}^2 + {BP_n}^2 + {DP_n}^2\right)\right) + \left(1/\left({AP_n}^2 + {BP_n}^2 + {EP_n}^2\right)\right) + \left(1/\left({AP_n}^2 + {CP_n}^2 + {DP_n}^2\right)\right) + \left(1/\left({AP_n}^2 + {CP_n}^2 + {EP_n}^2\right)\right)} \\
&\quad + \frac{\left(Y_6/\left({AP_n}^2 + {DP_n}^2 + {EP_n}^2\right)\right) + \left(Y_7/\left({BP_n}^2 + {CP_n}^2 + {DP_n}^2\right)\right) + \left(Y_8/\left({BP_n}^2 + {CP_n}^2 + {EP_n}^2\right)\right) + \left(Y_9/\left({BP_n}^2 + {DP_n}^2 + {EP_n}^2\right)\right) + \left(Y_{10}/\left({CP_n}^2 + {DP_n}^2 + {EP_n}^2\right)\right)}{+\left(1/\left({AP_n}^2 + {DP_n}^2 + {EP_n}^2\right)\right) + \left(1/\left({BP_n}^2 + {CP_n}^2 + {DP_n}^2\right)\right) + \left(1/\left({BP_n}^2 + {CP_n}^2 + {EP_n}^2\right)\right) + \left(1/\left({BP_n}^2 + {DP_n}^2 + {EP_n}^2\right)\right) + \left(1/\left({CP_n}^2 + {DP_n}^2 + {EP_n}^2\right)\right)}
\end{aligned} \quad (9)$$

where

$$\frac{1/\left({AP_n}^2 + {BP_n}^2 + {CP_n}^2\right)}{\left(1/\left({AP_n}^2 + {BP_n}^2 + {CP_n}^2\right)\right) + \left(1/\left({AP_n}^2 + {BP_n}^2 + {DP_n}^2\right)\right) + \left(1/\left({AP_n}^2 + {BP_n}^2 + {EP_n}^2\right)\right) + \left(1/\left({AP_n}^2 + {CP_n}^2 + {DP_n}^2\right)\right) + \left(1/\left({AP_n}^2 + {CP_n}^2 + {EP_n}^2\right)\right)} \quad (10)$$
$$+ \frac{1}{\left({AP_n}^2 + {DP_n}^2 + {EP_n}^2\right)} + \frac{1}{\left({BP_n}^2 + {CP_n}^2 + {DP_n}^2\right)} + \frac{1}{\left({BP_n}^2 + {CP_n}^2 + {EP_n}^2\right)} + \frac{1}{\left({BP_n}^2 + {DP_n}^2 + {EP_n}^2\right)} + \frac{1}{\left({CP_n}^2 + {DP_n}^2 + {EP_n}^2\right)}$$

etc. are the weighting coefficients.

3.2.3. Accuracy Evaluation. The reference value of the tree position was also measured and converted into the *xoy* plane coordinate system. First, the DBH was measured at 1.3 m using tape. Then, half of the tree DBH values were added to the reference and estimated position values of the plane coordinates in the *y*-axis and *x*-axis directions, respectively.

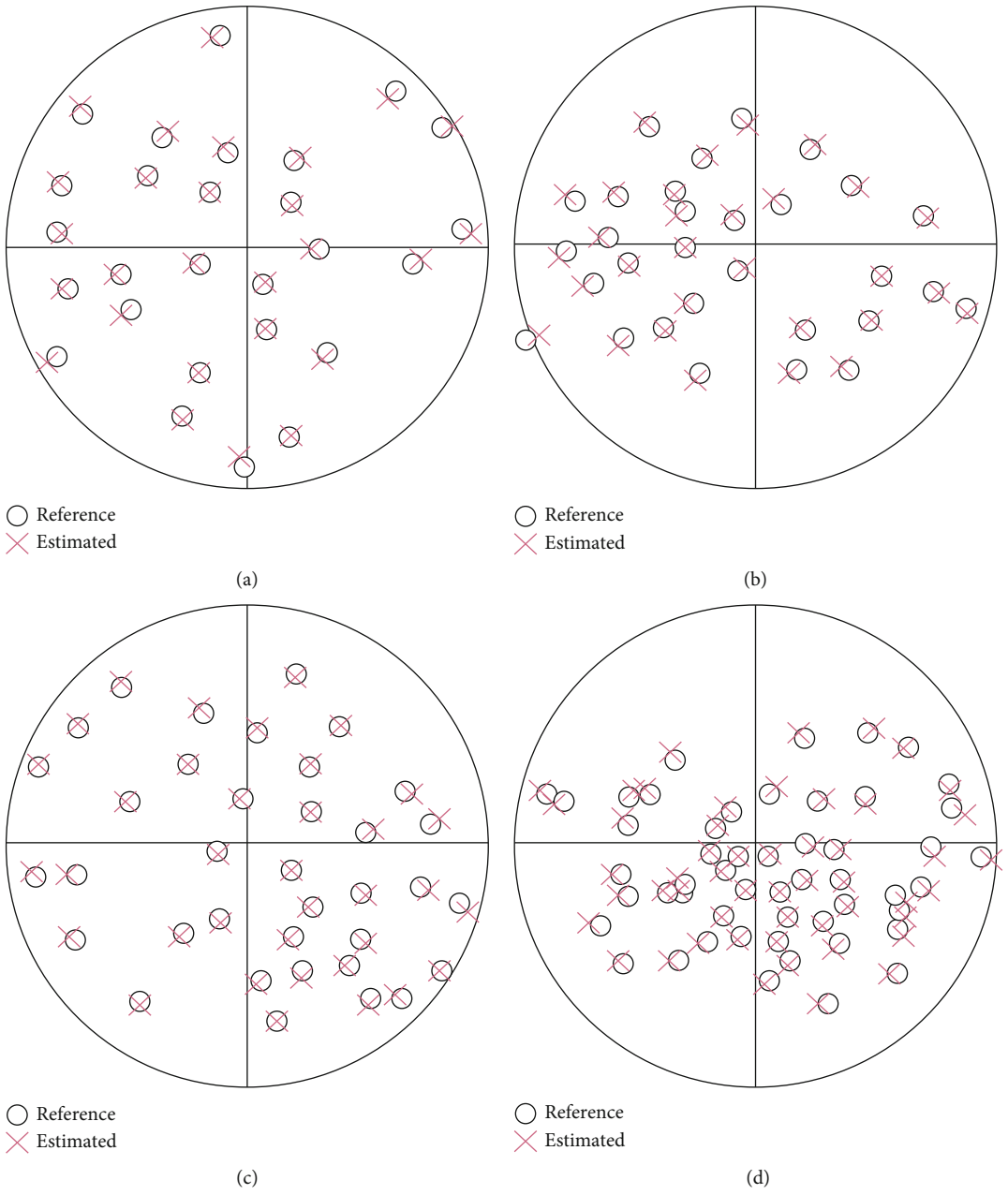

Figure 11: Continued.

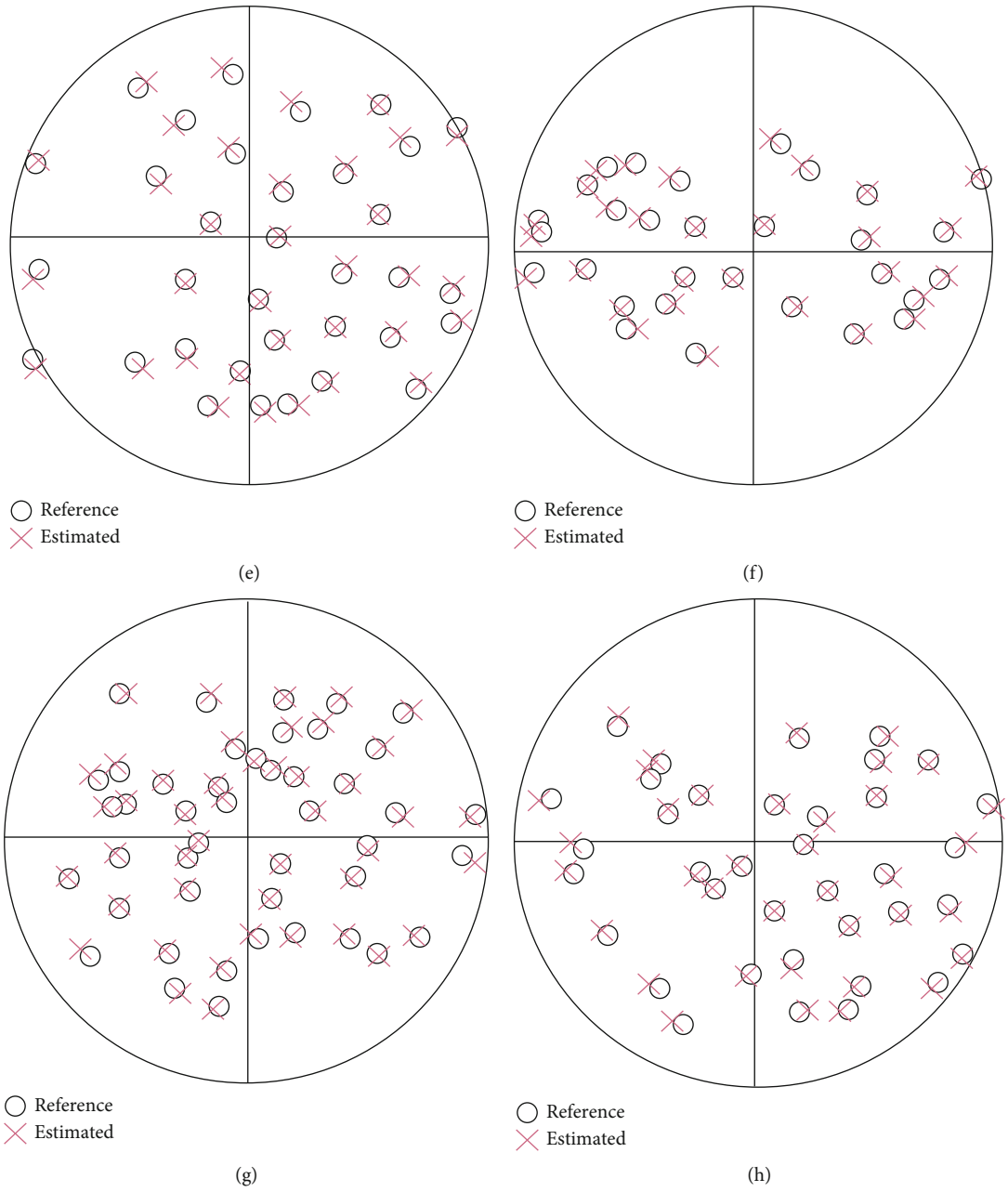

Figure 11: Continued.

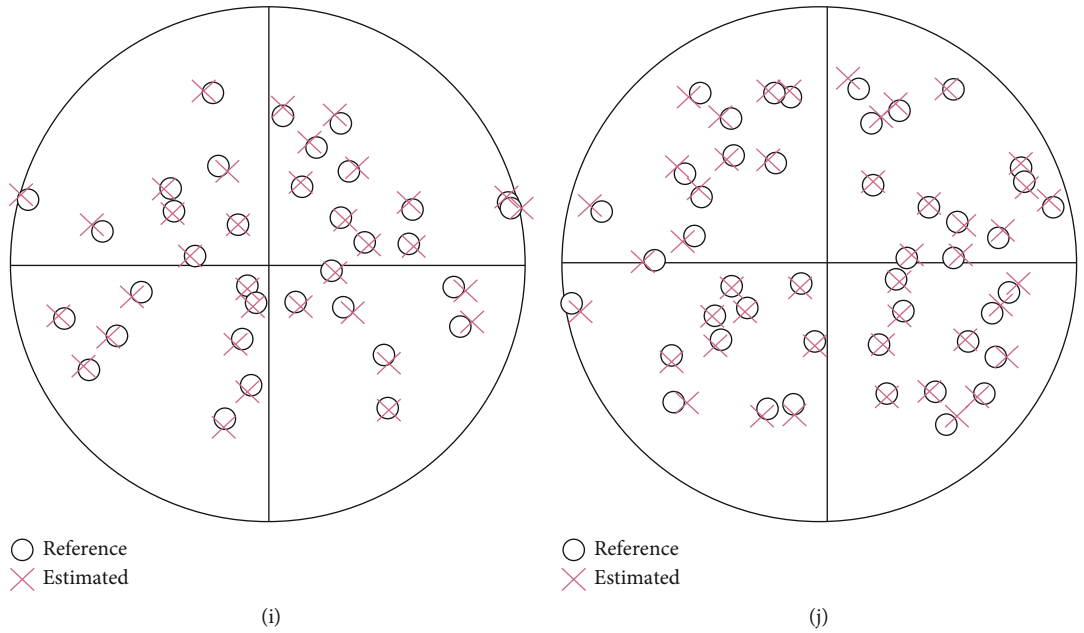

Figure 11: Comparisons of estimated and reference points: (a) plot 1; (b) plot 2; (c) plot 3; (d) plot 4; (e) plot 5; (f) plot 6; (g) plot 7; (h) plot 8; (i) plot 9; (j) plot 10.

Table 3: Accuracy in the x-axis and y-axis directions estimated by the device.

Plot	X (cm)		Y (cm)	
	BIAS	RMSE	BIAS	RMSE
1	-4.85	20.79	4.11	22.41
2	-3.97	24.10	2.23	21.09
3	-3.37	37.33	5.28	33.27
4	4.46	32.58	2.61	34.80
5	-6.99	29.19	-1.22	30.48
6	-8.05	27.85	2.74	27.90
7	-2.22	27.19	0.77	30.76
8	-6.39	28.50	1.35	30.02
9	-6.41	32.07	3.98	30.60
10	-1.65	24.34	9.34	23.93
Total	-3.94	28.39	3.36	28.53

Table 4: Summary statistics of the error of the distance between estimated and reference points.

Plot	Ed (cm)			
	Mean	Max	Min	Std
1	26.63	58.53	1.39	15.01
2	29.28	59.79	1.03	12.97
3	46.63	73.55	5.27	18.05
4	43.36	80.65	12.16	19.81
5	37.86	82.73	4.33	18.66
6	35.57	77.81	8.92	17.01
7	37.54	63.60	6.03	16.63
8	37.49	77.11	7.64	17.55
9	40.72	81.30	10.75	17.52
10	31.38	71.01	8.79	13.44
Total	36.13	82.73	1.03	16.67

According to Equations (11), (12), and (13), the bias, root mean square error (RMSE), and straight-line distance error between the estimation point and the reference point on the x- and y-axes were calculated separately to evaluate the accuracy of the method:

$$\text{BIAS} = \frac{\sum_{i=1}^{n}(d_i - D_{ir})}{n}, \tag{11}$$

$$\text{RMSE} = \sqrt{\frac{\sum_{i=1}^{n}(d_i - D_{ir})^2}{n}}, \tag{12}$$

$$\text{Ed} = \sqrt{(X_i - X_{ir})^2 + (Y_i - Y_{ir})^2}, \tag{13}$$

where d_i is the ith measured value, D_{ir} is the ith reference value, X_i and Y_i are the ith estimates on the x-axis and y-axis, respectively, X_{ir} and Y_{ir} are the ith reference values on the x-axis and y-axis, respectively, and n is the total number of measurements.

3.2.4. Efficiency Evaluation. To evaluate the efficiency of measurement, the times required for traditional and device measurement were recorded. To ensure that the two methods worked in the same order, the trees were numbered prior to measurement. Using the theodolite with a laser rangefinder measurement requires two people in a group: one stands in the middle of the circle to operate the theodolite with laser rangefinder correctly and then records the distances and angles from the center of the

Table 5: Comparison of work efficiency.

Method	Number of surveyors	Times of measurement	Total time (s)	Mean time (s)
Theodolite with a laser rangefinder	2	1	25880.96	69.76
UWB device	1	1	8299.27	22.37

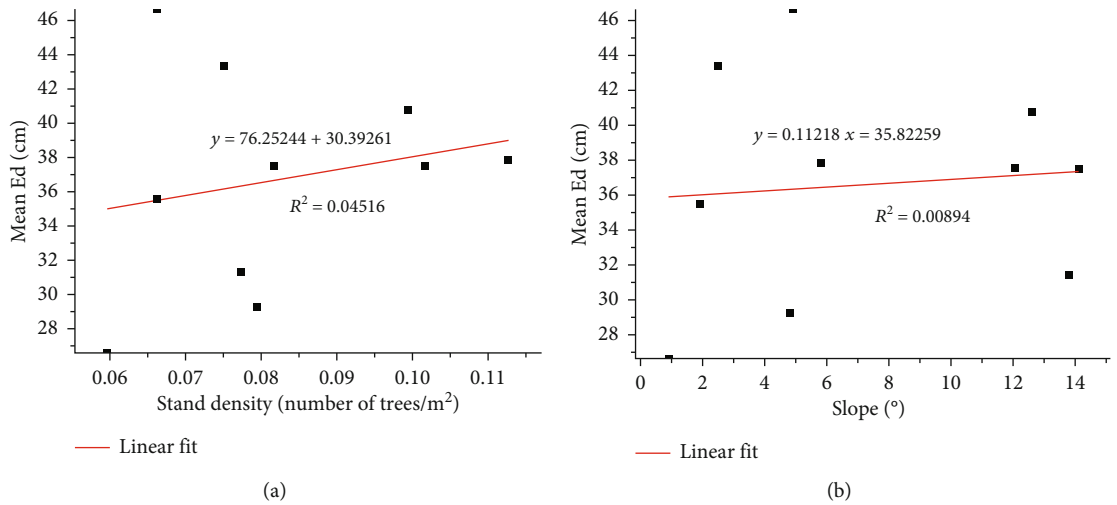

Figure 12: Scatter plot between mean Ed and (a) stand density and (b) slope.

circle plot (the angles to due north) and the other holds a surveyor's pole at the tree position. After the measurement is completed, the data recorded on a paper form is entered into the computer. When using the device for measurements, one person performs ranging and recording integration.

4. Results

4.1. Accuracy of Position Measurement. The error distribution and comparison results between the estimated points and the reference points are shown in Figures 10 and 11, respectively. The statistical results of the coordinate accuracy on the x-axis and y-axis and the statistical results of the linear distance errors between the estimated point and the reference point are shown in Tables 3 and 4, respectively. The results showed that the bias, RMSE, and total bias on the x- and y -axes were −8.05 to 4.46 cm and −1.22 cm to 9.34 cm, 20.79 to 37.33 cm and 21.09 to 34.80 cm, and −3.94 and 3.36 cm, respectively (Table 3). The mean Ed was 36.13 cm, the maximum Ed was 82.73 cm, the minimum Ed was 1.03 cm, and the standard deviation was 16.67 cm (Table 4). The Ed range of the estimated points and the reference points in the xoy plane was 0 cm to 83 cm (Figure 10). Systematic error was observed between the estimated values and the reference values of each sample plot, although the total error was small (Figure 11). The mean Ed values in the sample plots from 1 to 6 and 7 to 10 were 36.55 cm and 36.78 cm, respectively, indicating that the slope of the measured sample plot had no significant influence on the location.

4.2. Efficiency of Position Measurement. The measurement times of the two methods are shown in Table 5. The results showed that the mean measurement times were 22.37 and 69.76 s using the device and traditional methods, respectively. The measurement efficiency can be increased more than threefold using the proposed method.

5. Discussion

Tree position measurement is an important task in forest resource surveys. In recent years, a large number of tree location devices and methods have been reported. The Haglöf Postex® Laser, which was similar to the developed device, used an ultrasonic solution for position measurements, but ultrasound had a short measurement range and was not suitable for measurements of large sample plots. In addition, the device was not cheap [11]. Oveland et al. [18] proposed a positioning scheme under relatively rough conditions using a moving terrestrial laser scanner and GNSS. However, due to the serious attenuation of GNSS signals under the crown, this scheme was not suitable for accurate tree positioning; moreover, the devices were also expensive. Gollob et al. [30] located tree trunk positions using a terrestrial laser scanner; however, the data processing was complex and the device was hard to carry and thus was unsuitable for widespread application in forestry. Fan et al. [33] estimated tree position using an RGB-D smartphone combined with the simultaneous localization and mapping (SLAM) algorithm, and the results showed that the biases on the x- and y-axes were the same (-0.12 to 0.13 m) while the RMSEs were 0.09 m to 0.17 m and 0.07 m to 0.17 m, respectively. Although this method had high positioning accuracy, it was highly susceptible to the influence of the surrounding environment and requires professional training to handle the complex point

cloud processing. Our device only used the RSSI algorithm and pentagonal localization algorithm, which could be run on STC15 (8-bit) microprocessors (price under $1) and had much lower complexity in both time and space.

In this study, we designed a tree positioning device (cost of approximately $250) using UWB sensors. To test the estimation accuracy, we chose 10 circular plots with a diameter of 24 m to carry out our experiment. The results showed that the x- and y-axes had biases of -8.05 to 4.46 cm and -1.22 cm to 9.34 cm, respectively. The RMSEs of the x- and y-axes were 20.79 to 37.33 cm and 21.09 to 34.80 cm, respectively (Table 3). The mean error (Ed) and standard deviation of the distance between the estimated points and the reference points were 36.13 and 16.67 cm, respectively (Table 4). In terms of measurement efficiency, the traditional method required two people to complete the work and the data need to be recorded manually. However, the proposed device could be operated by one person and equipped with corresponding host computer software that integrated data measurement, recording, and uploading. The mean times required by the traditional method and the proposed device were 69.76 s and 22.37 s, respectively (Table 5). The device could locate trees accurately, and the measuring efficiency could be improved by more than three times.

Although the proposed device accurately located trees, considerable improvements remain to be made. For example, the maximum distance between the two anchor points was 2 m, which precludes the device's deployment in sample plots with high stand density. Note that using the device to measure the tree position may be affected by the plot environment. Compared with the slope, the stand density was more influential (Figure 12 and Table 2). In future research, we will ensure the positioning precision to reduce the size of the base station and conduct deeper research in a variety of complex sample environments to identify methods that can improve the positioning accuracy and reduce the impact of the plot environment on ranging.

6. Conclusions

This paper reports a novel device that uses UWB sensor technology to locate trees. It has a delicate mechanical structure and is based on trilateration and quadrilateral localization. A pentagonal localization algorithm was constructed to precisely locate trees. Through the host computer software, it performs data measurement, recording, and uploading integration, which increases the measurement efficiency more than three times compared to the traditional method.

Data Availability

The data used to support the findings of this study are available from the corresponding author upon request.

Conflicts of Interest

The authors declare no conflict of interest.

Acknowledgments

This work was financially supported by Science and Technology Program of Zhejiang Province (2018C02013) and New Seedling Talent Project of Zhejiang Province (2020R412045).

References

[1] M. Mokroš, J. Výbošťok, J. Tomaštík et al., "High precision individual tree diameter and perimeter estimation from close-range photogrammetry," *Forests*, vol. 9, p. 696, 2018.

[2] M. Mokroš, X. Liang, P. Surový et al., "Evaluation of close-range photogrammetry image collection methods for estimating tree diameters," *ISPRS International Journal of Geo-Information*, vol. 7, no. 3, p. 93, 2018.

[3] J. A. Kershaw, M. J. Ducey, T. W. Beers, and B. Husch, *Forest mensuration*, John Wiley & Sons, Ltd., Chichester, UK, 2016.

[4] H. Kramer and A. Akça, *Leitfaden zur Waldmesslehre*, J. D. Sauerländers Verlag, Bad Orb, Germany, 2008.

[5] J. B. Kuffman, V. B. Arifanti, I. Basuki et al., *Protocols for the Measurement, Monitoring, and Reporting of Structure, Biomass, Carbon Stocks and Greenhouse Gas Emissions in Tropical Peat Swamp Forests*, Center for International Forestry Research (CIFOR), Bogor, Indonesia, 2017.

[6] M. Köhl, S. Magnussen, and M. Marchetti, *Sampling Methods, Remote Sensing and GIS Multiresource Forest Inventory; Tropical Forestry*, Springer Berlin Heidelberg, Berlin, Heidelberg, 2006.

[7] X. Liang, A. Kukko, J. Hyyppä et al., "In-situ measurements from mobile platforms: an emerging approach to address the old challenges associated with forest inventories," *ISPRS Journal of Photogrammetry and Remote Sensing*, vol. 143, pp. 97–107, 2018.

[8] X. Liang, V. Kankare, J. Hyyppä et al., "Terrestrial laser scanning in forest inventories," *ISPRS Journal of Photogrammetry and Remote Sensing*, vol. 115, pp. 63–77, 2016.

[9] X. Liang, J. Hyyppä, H. Kaartinen et al., "International benchmarking of terrestrial laser scanning approaches for forest inventories," *ISPRS Journal of Photogrammetry and Remote Sensing*, vol. 144, pp. 137–179, 2018.

[10] T. Ritter, M. Schwarz, A. Tockner, F. Leisch, and A. Nothdurft, "Automatic mapping of forest stands based on three-dimensional point clouds derived from terrestrial laser-scanning," *Forests*, vol. 8, no. 8, p. 265, 2017.

[11] HaglöfSweden, *Haglöf Postex® Laser*, 2021, https://haglofsweden.com/project/postex-laser/.

[12] J. Ryding, E. Williams, M. Smith, and M. Eichhorn, "Assessing handheld mobile laser scanners for forest surveys," *Remote Sensing*, vol. 7, no. 1, pp. 1095–1111, 2015.

[13] S. Bauwens, H. Bartholomeus, K. Calders, and P. Lejeune, "Forest inventory with terrestrial LiDAR: a comparison of static and hand-held mobile laser scanning," *Forests*, vol. 7, no. 12, p. 127, 2016.

[14] C. Cabo, S. Del Pozo, P. Rodríguez-Gonzálvez, C. Ordóñez, and D. González-Aguilera, "Comparing terrestrial laser scanning (TLS) and wearable laser scanning (WLS) for individual tree modeling at plot level," *Remote Sensing*, vol. 10, no. 4, p. 540, 2018.

[15] B. Del Perugia, F. Giannetti, G. Chirici, and D. Travaglini, "Influence of scan density on the estimation of single-tree attributes by

hand-held mobile laser scanning," *Forests*, vol. 10, no. 3, p. 277, 2019.

[16] S. Chen, H. Liu, Z. Feng, C. Shen, and P. Chen, "Applicability of personal laser scanning in forestry inventory," *PLoS One*, vol. 14, no. 2, article e0211392, 2019.

[17] A. Kukko, R. Kaijaluoto, H. Kaartinen, V. V. Lehtola, A. Jaakkola, and J. Hyyppä, "Graph SLAM correction for single scanner MLS forest data under boreal forest canopy," *ISPRS Journal of Photogrammetry and Remote Sensing*, vol. 132, pp. 199–209, 2017.

[18] I. Oveland, M. Hauglin, T. Gobakken, E. Næsset, and I. Maalen-Johansen, "Automatic estimation of tree position and stem diameter using a moving terrestrial laser scanner," *Remote Sensing*, vol. 9, no. 4, p. 350, 2017.

[19] X. Liang and J. Hyyppä, "Automatic stem mapping by merging several terrestrial laser scans at the feature and decision levels," *Sensors*, vol. 13, no. 2, pp. 1614–1634, 2013.

[20] P. J. Watt and D. N. M. Donoghue, "Measuring forest structure with terrestrial laser scanning," *International Journal of Remote Sensing*, vol. 26, no. 7, pp. 1437–1446, 2005.

[21] C. Vonderach, T. Vögtle, P. Adler, and S. Norra, "Terrestrial laser scanning for estimating urban tree volume and carbon content," *International Journal of Remote Sensing*, vol. 33, no. 21, pp. 6652–6667, 2012.

[22] J. Liu, X. Liang, J. Hyyppä et al., "Automated matching of multiple terrestrial laser scans for stem mapping without the use of artificial references," *International Journal of Applied Earth Observation and Geoinformation*, vol. 56, pp. 13–23, 2017.

[23] T. Ritter and A. Nothdurft, "Automatic assessment of crown projection area on single trees and stand-level, based on three-dimensional point clouds derived from terrestrial laser-scanning," *Forests*, vol. 9, no. 5, p. 237, 2018.

[24] L. M. Moskal and G. Zheng, "Retrieving forest inventory variables with terrestrial laser scanning (TLS) in urban heterogeneous forest," *Remote Sensing*, vol. 4, no. 1, pp. 1–20, 2012.

[25] X. Liang, P. Litkey, J. Hyyppa, H. Kaartinen, M. Vastaranta, and M. Holopainen, "Automatic stem mapping using single-scan terrestrial laser scanning," *IEEE Transactions on Geoscience and Remote Sensing*, vol. 50, no. 2, pp. 661–670, 2012.

[26] M. Béland, J.-L. Widlowski, R. A. Fournier, J.-F. Côté, and M. M. Verstraete, "Estimating leaf area distribution in savanna trees from terrestrial LiDAR measurements," *Agricultural and Forest Meteorology*, vol. 151, no. 9, pp. 1252–1266, 2011.

[27] H. M. Rizeei, H. Z. M. Shafri, M. A. Mohamoud, B. Pradhan, and B. Kalantar, "Oil palm counting and age estimation from worldview-3 imagery and LiDAR data using an integrated OBIA height model and regression analysis," *Journal of Sensors*, pp. 1–13, 2018.

[28] S. Srinivasan, S. Popescu, M. Eriksson, R. Sheridan, and N.-W. Ku, "Terrestrial laser scanning as an effective tool to retrieve tree level height, crown width, and stem diameter," *Remote Sensing*, vol. 7, no. 2, pp. 1877–1896, 2015.

[29] P. Pueschel, G. Newnham, G. Rock, T. Udelhoven, W. Werner, and J. Hill, "The influence of scan mode and circle fitting on tree stem detection, stem diameter and volume extraction from terrestrial laser scans," *ISPRS Journal of Photogrammetry and Remote Sensing*, vol. 77, pp. 44–56, 2013.

[30] C. Gollob, T. Ritter, C. Wassermann, and A. Nothdurft, "Influence of scanner position and plot size on the accuracy of tree detection and diameter estimation using terrestrial laser scanning on forest inventory plots," *Remote Sensing*, vol. 11, no. 13, article 1602, 2019.

[31] J. Hyyppä, J.-P. Virtanen, A. Jaakkola, X. Yu, H. Hyyppä, and X. Liang, "Feasibility of Google Tango and Kinect for crowdsourcing forestry information," *Forests*, vol. 9, p. 6, 2018.

[32] J. Tomaštík, Š. Saloň, D. Tunák, F. Chudý, and M. Kardoš, "Tango in forests - an initial experience of the use of the new Google technology in connection with forest inventory tasks," *Computers and Electronics in Agriculture*, vol. 141, pp. 109–117, 2017.

[33] Y. Fan, Z. Feng, A. Mannan, T. Ullah Khan, C. Shen, and S. Saeed, "Estimating tree position, diameter at breast height, and tree height in real-time using a mobile phone with RGB-D SLAM," *Remote Sensing*, vol. 10, no. 11, article 1845, 2018.

[34] T. Mikita, P. Janata, and P. Surovỳ, "Forest stand inventory based on combined aerial and terrestrial close-range photogrammetry," *Forests*, vol. 7, no. 12, p. 165, 2016.

[35] L. Sun, L. Fang, L. Tang, and J. Liu, "Developing portable system for measuring diameter at breast height," *Journal of Beijing Forestry University*, vol. 40, pp. 82–89, 2018.

[36] P. Surový, A. Yoshimoto, and D. Panagiotidis, "Accuracy of reconstruction of the tree stem surface using terrestrial close-range photogrammetry," *Remote Sensing*, vol. 8, no. 2, p. 123, 2016.

[37] M. Forsman, N. Börlin, and J. Holmgren, "Estimation of tree stem attributes using terrestrial photogrammetry with a camera rig," *Forests*, vol. 7, no. 12, p. 61, 2016.

[38] S. Sun, J. Hu, J. Li, R. Liu, M. Shu, and Y. Yang, "An INS-UWB based collision avoidance system for AGV," *Algorithms*, vol. 12, no. 2, p. 40, 2019.

[39] C. Baard, Y. Liu, and N. Nikolova, "Ultra-wideband low-cost high-efficiency cavity-backed compound spiral antenna," *Electronics*, vol. 9, no. 9, article 1399, 2020.

[40] J. Jung, Y. Choi, and Y. Kwon, "Location-aware point-to-point RPL in indoor IR-UWB networks," *Electronics*, vol. 9, no. 5, p. 861, 2020.

[41] X. Hu, Z. Luo, and W. Jiang, "AGV localization system based on ultra-wideband and vision guidance," *Electronics*, vol. 9, no. 3, p. 448, 2020.

[42] M.-H. Weng, F.-Z. Zheng, H.-Z. Lai, and S.-K. Liu, "Compact ultra-wideband bandpass filters achieved by using a stub-loaded stepped impedance resonator," *Electronics*, vol. 9, no. 2, p. 209, 2020.

[43] S. Monica and G. Ferrari, "Impact of the number of beacons in PSO-based auto-localization in UWB networks," in *Applications of Evolutionary Computation; Lecture Notes in Computer Science, Volume 7835*, pp. 42–51, Springer, Berlin/Heidelberg, Germany, 2013.

[44] S. Krishnan, P. Sharma, Z. Guoping, and O. H. Woon, "A UWB based localization system for indoor robot navigation," in *2007 IEEE International Conference on Ultra-Wideband*, pp. 77–82, Singapore, September 2007.

[45] S. Monica and F. Bergenti, "A comparison of accurate indoor localization of static targets via WiFi and UWB ranging," in *Trends in Practical Applications of Scalable Multi-Agent Systems; Lecture Notes in Computer Science, Volume 9662*, pp. 111–123, Springer, Cham, Switzerland, 2016.

[46] R. Matteo, V. D. V. Samuel, S. Heidi, and E. De Poorter, "Analysis of the scalability of UWB indoor localization solutions for high user densities," *Sensors*, vol. 18, article 1875, 2018.

[47] H. Xiaoping, W. Fei, Z. Jian, Z. Hu, and J. Jin, "A posture recognition method based on indoor positioning technology," *Sensors*, vol. 19, article 1464, 2019.

[48] J. He, Y. Wu, S. Duan et al., "Model of human body influence on UWB ranging error," *The Journal of Communication*, vol. 38, pp. 58–66, 2017.

[49] S. Juri, S. Volker, S. Norbert, M. Arensa, and U. Hugentobler, "Decawave UWB clock drift correction and powerself-calibration," *Sensors*, vol. 19, article 2942, 2019.

[50] S. Hamdoun, A. Rachedi, and A. Benslimane, "Comparative analysis of RSSI-based indoor localization when using multiple antennas in wireless sensor networks," in *2013 International Conference on Selected Topics in Mobile and Wireless Networking (MoWNeT)*, pp. 146–151, Montreal, QC, Canada, August 2013.

[51] X. Zhu and Y. Feng, "RSSI-based algorithm for indoor localization," *Communications and Network*, vol. 5, no. 2, pp. 37–42, 2013.

[52] V. Barral, C. J. Escudero, J. A. García-Naya, and R. Maneiro-Catoira, "NLOS identification and mitigation using low-cost UWB devices," *Sensors*, vol. 19, no. 16, article 3464, 2019.

[53] A. Harter, A. Hopper, P. Steggles, A. Ward, and P. Webster, "The anatomy of a context-aware application," *Wireless Networks*, vol. 8, no. 2/3, pp. 187–197, 2002.

[54] M. Stefania and B. Federico, "Hybrid indoor localization using WiFi and UWB technologies," *Electronics*, vol. 8, p. 334, 2019.

[55] J. Wen, J. Jin, and H. Yuan, "Quadrilateral localization algorithm for wireless sensor networks," *Transducer and Microsystem Technologies*, vol. 27, pp. 108–110, 2008.

[56] H. Gao and L. Xu, "Tightly-coupled vehicle positioning method at intersections aided by UWB," *Sensors*, vol. 19, no. 13, article 2867, 2019.

[57] L. Sun, L. Fang, Y. Weng, and S. Zheng, "An integrated method for coding trees, measuring tree diameter, and estimating tree positions," *Sensors*, vol. 20, p. 144, 2020.